

Double Check My Desired Return: Transformer with Target Alignment for Offline Reinforcement Learning

Yue Pei^a, Hongming Zhang^b, Chao Gao^c, Martin Müller^b, Mengxiao Zhu^d,
Hao Sheng^e, Ziliang Chen^f, Liang Lin^f, Haogang Zhu^{e,*}

^a*School of Artificial Intelligence, Beihang University, Beijing, China*

^b*Department of Computing Science and Amii, University of Alberta, Edmonton, Canada*

^c*Edmonton Research Center, Huawei Canada, Edmonton, Canada*

^d*School of Artificial Intelligence and Computer Science, North China University of Technology, Beijing, China*

^e*School of Computer Science and Engineering, Beihang University, Beijing, China*

^f*Research Institute of Multiple Agents and Embodied Intelligence, Peng Cheng Laboratory, Shenzhen, China*

Abstract

Offline reinforcement learning (RL) has achieved significant advances in domains such as robotic control, autonomous driving, and medical decision-making. Most existing methods primarily focus on training policies that maximize cumulative returns from a given dataset. However, many real-world applications require precise control over policy performance levels, rather than simply pursuing the best possible return. Reinforcement learning via supervised learning (RvS) frames offline RL as a sequence modeling task, enabling the extraction of diverse policies by conditioning on different desired returns. Yet, existing RvS-based transformers, such as Decision Transformer (DT), struggle to reliably align the actual achieved returns with specified target returns, especially when interpolating within underrepresented returns or extrapolating beyond the dataset. To address this limitation, we propose *Doctor*, a novel approach that **Double Checks** the Transformer with target alignment for **Offline RL**. *Doctor* integrates the strengths of supervised learning (SL) and temporal difference (TD) learning by jointly optimizing the action prediction and value estimation. During inference, *Doctor* introduces a double-check mechanism: actions are first sampled around the desired target returns and then validated with value functions. This en-

*Corresponding author.

sures more accurate alignment between predicted actions and desired target returns. We evaluate *Doctor* on the D4RL and EpiCare benchmarks, demonstrating aligned control yields stronger performance and tunable expertise, showing its effectiveness in a wide range of tasks.

Keywords:

Offline Reinforcement Learning, Transformer, Target Alignment, Decision and Control

1. Introduction

In recent years, offline reinforcement learning (RL) [1] has made remarkable progress in various domains, including robotic control [2, 3], autonomous driving [4], and medical decision-making [5, 6]. Most existing methods primarily aim to maximize the cumulative rewards, seeking to extract the best possible policy from a given offline dataset [7].

However, in many practical applications, it is necessary to precisely control the agent’s skill level in order to achieve different performance targets, rather than merely extracting the best-performing policy. For instance, AI clinicians need to satisfy personalized medicine requirements according to individual patient profiles [8], and educational AI assistants must dynamically adapt content and difficulty to match the abilities of different students [9, 10]. In game AI, diverse NPC skill levels are crucial for a rich and engaging gameplay experience [11].

Recent approaches have formulated offline RL as a sequence modeling problem analogous to large-scale language modeling, learning policies through supervised learning [12, 13]. This paradigm, known as reinforcement learning via supervised learning (RvS) [14], predicts actions for each state in a

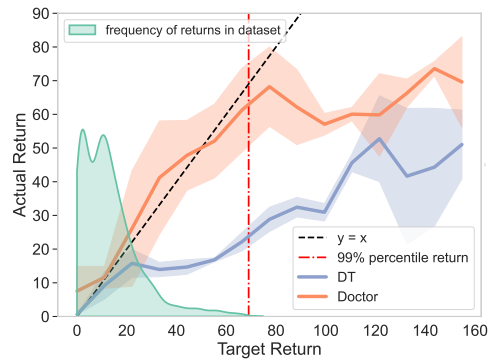


Figure 1: The actual returns achieved by *Doctor* and Decision Transformer (DT) conditioned on a wide range of target returns on the Hopper-Medium-Replay dataset. *Doctor* demonstrates significantly better alignment than DT, not only for well-supported returns within the dataset but also for extrapolated returns beyond the dataset.

supervised manner, conditioned on historical trajectories along with a target return prompt. By specifying the desired return as input, the learned transformer model is expected to output actions that achieve that particular return level. Thus, RvS approaches enable the adjustment of policy by varying the target return prompt.

However, transformers trained via RvS typically struggle to align the achieved return with the specified target return. As illustrated in Figure 1, Decision Transformer (DT) [12], an RvS-based method, only achieves alignment within well-supported returns in the dataset. DT struggles to interpolate effectively across underrepresented return regions (left side of the dashed red line), and it also fails to reliably extrapolate to higher returns beyond those observed in the training data (right side of the dashed red line). This limitation suggests that training solely with RvS is insufficient for learning policies whose actual returns closely match specified targets. Therefore, developing methods that explicitly perform target alignment is essential to accurately extract desired policies from an offline dataset, thus significantly benefiting a variety of applications. Nonetheless, existing work addressing precise target alignment in offline RL remains relatively limited.

To fill this research gap, we aim to address the target alignment problem for RvS transformers, namely, achieving aligned control that calibrates policy behavior across expertise levels. We propose a novel method, *Doctor*, which **Double Checks the Transformer with target alignment for Offline RL**. *Doctor* integrates the strengths of supervised learning and temporal difference learning by jointly optimizing the action prediction and value estimation. Supervised learning stabilizes the prediction of actions conditioned on target returns, while temporal difference learning adds stitching capability to the transformer and plays a critical role in alignment. At inference time, we introduce a double-check mechanism that first generates a diverse set of candidate actions by scaling outputs conditioned on sampled returns and then estimates these actions using learned value functions, selecting the action whose associated value prediction most closely aligns with the specified target. This mechanism effectively broadens the return coverage and improves alignment for underrepresented or unseen target returns. In summary, our contributions are as follows.

(1) We propose a novel method, *Doctor*, that integrates the strengths of supervised learning and temporal difference learning in a transformer for offline RL. By jointly optimizing supervised trajectory reconstruction and temporal-difference value estimation, *Doctor* demonstrates the ability

to interpolate across underrepresented return ranges and extrapolate beyond dataset-supported regions.

(2) *Doctor* introduces a novel double-check mechanism at inference time that significantly enhances target alignment. By generating multiple actions conditioned on sampled returns and validating these candidates using value functions, this mechanism enhances the alignment between predicted actions and desired targets, enabling the extraction of policies with varying performance levels

(3) We empirically evaluate *Doctor* on offline RL benchmarks, including D4RL [15] and EpiCare [5], demonstrating superior target alignment both within and beyond the dataset. Furthermore, aligned control can translate to better return maximization performance. *Doctor* achieves competitive results compared to existing methods, showing its effectiveness in a wide range of tasks.

(4) We demonstrate that the precise target alignment enables accurate control over the expertise of the policy, providing benefits for RL applications. Specifically, on the dynamic treatment regime benchmark EpiCare, *Doctor* effectively modulates the aggressiveness of treatment policies, flexibly balancing therapeutic efficacy against adverse event risk.

2. Related Work

In this section, we review methods related to our approach and delineate the key distinctions between our method and these existing techniques.

Value Function Learning in Offline RL. Offline reinforcement learning only uses existing data collected by unknown policies without additional online data collection. One line of work is based on temporal difference (TD) learning [16, 17, 18, 19]. To constrain the distance between the learned policy and the behavior policy to avoid distributional shift, they use a conservative value function to estimate the value of actions either by adding a regularization term in TD learning [20, 21], or updating the value function in an in-sample manner [18, 22]. CQL [23] augments the standard Bellman error objective with a simple Q-value regularizer, such that the expected value of a policy under the learned Q-function lower-bounds its true value. Implicit Q-Learning (IQL) [18] estimates the value of the best available action at a given state with expectile regression, without ever directly querying the Q function for unseen actions. These methods aim to extract the best possible policy from the existing dataset. Unlike these approaches, *Doctor*'s target

alignment enables the model to perform at multiple skill levels, thereby benefiting offline RL.

Sequence Modeling based Methods for Offline RL. Another line of work is Reinforcement Learning via Supervised Learning (RvS). These methods cast offline RL as a conditional sequence modeling problem and learn a policy auto-regressively. Benefit from the inherent stability and scalability of SL, these methods bypasses the need for bootstrapping for long term credit assignment and avoids the “deadly triad” [17] known to destabilize RL. These approaches [24, 25, 26] commonly condition on goals and expect that the derived policy could be improved by feeding a high goal. DT [12] trains a transformer to autoregressively predict action sequences based on desired return and past trajectory. MTM [27] applies masked prediction to learn a generic and versatile model for prediction, representation, and control. To enhance transformers with stitching ability and recover the best policy from the dataset, recent approaches leverage Dynamic Programming [28, 29], exploit Q-values to guide actions [30], or incorporate Q-value regularization into transformers [31]. Although RvS tends to be stable, these methods struggle to align the actual return with the desired target return [32]. Therefore, our primary objective is explicit target alignment, enabling an offline-trained transformer to accurately perform at different skill levels.

3. Preliminaries

3.1. Offline Reinforcement Learning

Reinforcement learning (RL) [17] is a paradigm of agent learning via interaction. It can be modeled as a Markov Decision Process (MDP), a 5-tuple $\mathcal{M} = (\mathcal{S}, \mathcal{A}, \mathcal{R}, P, \gamma)$. \mathcal{S} denotes the state space, \mathcal{A} denotes the action space, $P(s'|s, a) : \mathcal{S} \times \mathcal{A} \times \mathcal{S} \rightarrow [0, 1]$ is the environment dynamics, $\mathcal{R}(s, a) : \mathcal{S} \times \mathcal{A} \rightarrow \mathbb{R}$ is the reward function which is bounded, $\gamma \in [0, 1]$ is the discount factor. Consider the finite horizon setting, the agent interacts with the environment for T steps. Denote the state, action and reward at timestep t as s_t , a_t and r_t , a trajectory is a sequence of states, actions and rewards $\tau := (s_0, a_0, r_0, s_1, a_1, r_1, \dots, s_T, a_T, r_T)$. The return at timestep t is defined as $R_t = \sum_{i=t}^T \gamma^{i-t} r_i$. The goal of an reinforcement learning agent is to learn an optimal policy π that maximizes the expected return $R_0 = \mathbb{E}_\pi[\sum_{i=0}^T \gamma^i r_i]$.

In offline RL, instead of interacting with the environment, the agent learns from a static dataset of trajectories $\mathcal{D} := \{\tau_j\}$ such as the D4RL benchmark [15]. The dataset is collected by either one or multiple unknown behav-

ior policies, and the agent’s goal is to learn a policy based on the dataset that performs well in the environment. Several recent offline-RL methods impose an in-sample constraint, learning Q-functions over the dataset’s state–action visitation:

$$Q(s, a) \leftarrow r + \gamma \max_{(s', a') \in \mathcal{D}} Q(s', a'). \quad (1)$$

For example, Implicit Q-Learning (IQL) [18] only bootstraps from actions seen in the dataset, avoiding value estimates on unseen actions and substantially reducing estimation error. This setting eliminates the need for online exploration, which is practical in scenarios where exploration is expensive or dangerous.

3.2. Reinforcement Learning via Supervised Learning.

The transformer model [33] is trained with a masked language modeling objective, where the model predicts the next token in the sequence given the previous tokens. Transformers have shown remarkable success in various tasks such as natural language processing and computer vision [34, 35]

Decision Transformer (DT) [12] applies transformers to offline RL. Different from offline RL methods based on temporal difference learning, DT models offline RL as a sequence modeling problem and learns a policy autoregressively by predicting the next action given the history trajectory conditioned on a target return. This set of approaches abstract offline RL as a sequence modeling problem and learns a policy via supervised learning (RvS). The K-step historical trajectory sequence τ_t consists of three modalities:

$$\tau_t = (R_{t-K+1}, s_{t-K+1}, a_{t-K+1}, \dots, R_t, s_t, a_t), \quad (2)$$

where R_t is the (discounted) return at time step t , s_t is the state, and a_t is the action. These methods condition on goals or target returns and expect that the derived policy could be improved when feeding a high-goal or large-return.

4. Method

In this section, we introduce our method, *Doctor*. We first introduce our model architecture and describe how the model is trained to predict value and actions. We then introduce a double-check mechanism at inference time to improve alignment. Figure 2 illustrates the overall framework.

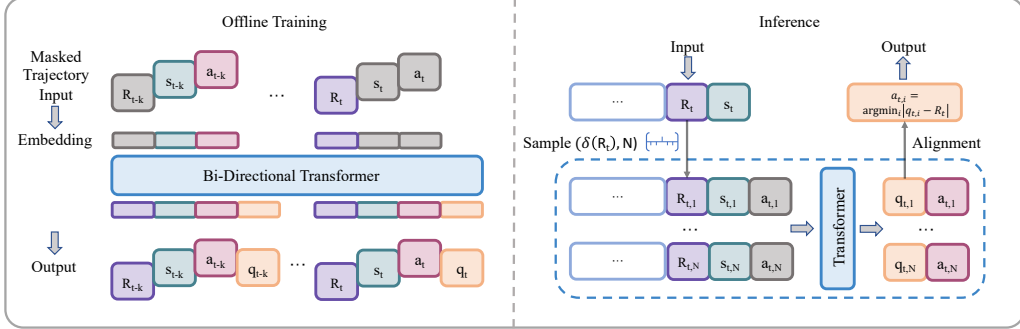


Figure 2: An overview of *Doctor*. **Left.** The training involves reconstructing the original trajectory and estimating the action-value from a partial, randomly masked trajectory. Returns, states and actions are fed into modality-specific embeddings and then processed by the transformers. The value heads estimate the action-value at each timestep. **Right.** At inference time, *Doctor* samples actions around the target return and validates them with the value head outputs to ensure alignment.

4.1. Model Architecture

Our model adopts an encoder-decoder architecture as a universal representation extractor. Both the encoder and decoder are bidirectional transformers, which are adept at capturing dependencies in sequential data. The task is based on sequence reconstruction from masked views [33, 36], where a random subset of the sequence is masked and the model is tasked with reconstructing the original trajectory.

This design choice is motivated by recent work [27] which demonstrated that bidirectional transformers trained with random and auto-regressive masking encourage the model to reconstruct missing tokens by leveraging the context of the unmasked sequence, enhancing the generalization. We expect this design to yield stronger interpolation when handling trajectories associated with underrepresented returns. Our experiments (Figure 4) confirm that the bidirectional transformer-based architecture achieves improved target alignment.

As illustrated in the left of Figure 2, we apply random and auto-regressive mask M to certain elements of the sequence,

$$M(\tau_t) = (R_{t-K+1}, _, a_{t-K+1}, _, s_{t-K+2}, _, \dots, _, s_T, _), \quad (3)$$

where the masked elements are denoted as $_$. The masked sequence $M(\tau_t)$ is then fed into the encoder-decoder architecture E and D to obtain the

last layer’s latent representation $\tau^z = D(E(M(\tau_t)))$. A linear layer for each modality is applied to the latent representation τ^z to predict the return, state, and action at each timestep.

Along with reconstructing the trajectory, the latent representation τ^z is also used to predict the action-value q_t at each timestep. τ^z integrates the information from multiple timesteps, which is beneficial for partial observability in RL tasks. And the action-value q_t endows the model with the ability to evaluate the return. At inference time, we fed the unmasked full trajectory into the model to obtain the predicted actions and action-values.

4.2. Training

Our training consists of two purposes: (1) reconstructing the original trajectory sequence from the masked input trajectory, which is a self-supervised learning task, and (2) learning the action-value q_t to enable the model for stitching and to improve the alignment, which is TD learning. We jointly optimize the model to minimize the reconstruction error and the TD error.

Denoting the learnable parameters of embeddings and the encoder-decoder as θ , inducing conditional probabilities as P_θ , the objective is to minimize the negative log-likelihood of the original trajectory sequence given the masked input:

$$\mathcal{L}_{\text{recon}}(\theta) = - \sum_{t=0}^T \left(\log P_\theta(R_t|M(\tau_t)) + \log P_\theta(s_t|M(\tau_t)) + \log P_\theta(a_t|M(\tau_t)) \right). \quad (4)$$

Besides reconstructing the trajectory, the model is also trained to predict the action-value q_t . Our Q function includes individual Q head at each timestep, corresponding to the state action pairs. It takes the latent trajectory representation τ^z as input and outputs action-value estimates. This enables the Q function to leverage the rich representations learned from the reconstruction task.

The goal of the Q function is to learn an optimal action-value function, aligning with target returns. To avoid querying the learned Q function on out-of-sample actions, we utilize the asymmetric least squares loss function [18]. Denote the learnable parameters of the Q function as ϕ . The learning loss is defined by:

$$\mathcal{L}_Q(\phi) = \sum_{t=0}^{T-1} L_2^\nu(r_t + \gamma Q_{\phi,t+1}(\tau^z, a_{t+1}) - Q_{\phi,t}(\tau^z, a_t)), \quad (5)$$

where r_t is the reward, γ is the discount factor, $Q_{\phi,t}$ and $Q_{\phi,t+1}$ are the Q functions at time step t and $t+1$, respectively. $L_2^\nu(u) = |\nu - \mathbf{1}(u < 0)|u^2$ is the asymmetric least squares loss function. For $\nu = 0.5$, the loss function is equivalent to the standard mean squared error loss. For $\nu > 0.5$, the loss function is asymmetric, which down-weights the contributions of values smaller than zero [37, 18, 38]. Eq. (1) can be approximated with $\tau \approx 1$.

We initialize Q functions Q_ϕ and train them jointly with the transformers. The overall objective is to minimize the sum of the reconstruction loss and the TD loss:

$$\mathcal{L}(\theta, \phi) = \mathcal{L}_{\text{recon}}(\theta) + \mathcal{L}_Q(\phi). \quad (6)$$

4.3. Inference Time Alignment

Given a tuple (R_t, s_t, a_t, q_t) , the return R_t represents the return in the dataset when taking action a_t at state s_t , while the action-value q_t reflects the expected return.

We expect there could be a gap between q_t and R_t . This gap presents the difference between policy evaluation of the unknown behavior policy that collected the dataset and the best possible policy after policy improvement. This motivates us to introduce a double-check mechanism during inference to ensure alignment between the predicted action and the target return.

Formally, given the current state s_t , denote R_t as the desired target return at timestep t . We define $\delta(R_t) := \{R : |R - R_t| \leq \delta\}$ as the set of returns within a distance δ from R_t . We sample N returns from $\delta(R_t)$ uniformly,

$$\{R_{t,1}, R_{t,2}, \dots, R_{t,N}\} \sim \text{Unif}(\delta(R_t), N), \quad (7)$$

and construct N trajectories by assigning $R_{t,i}$ to replace R_t in the original trajectory. We then feed these N trajectories into the transformer model:

$$\underbrace{\left\{ \begin{array}{c} (R_{t-K+1,i}, s_{t-K+1,i}, a_{t-K+1,i}) \\ \dots \\ (R_{t,i}, s_{t,i}, _) \end{array} \right\}}_{\text{input trajectories}} \xrightarrow{\quad} \underbrace{\left\{ \begin{array}{c} (R_{t-K+1,i}, s_{t-K+1,i}, a_{t-K+1,i}, q_{t-K+1,i}) \\ \dots \\ (R_{t,i}, s_{t,i}, a_{t,i}, q_{t,i}) \end{array} \right\}}_{\text{output trajectories}}^N, \quad (8)$$

where we obtain N predicted actions $\{a_{t,1}, a_{t,2}, \dots, a_{t,N}\}$ and their corresponding action-values $\{q_{t,1}, q_{t,2}, \dots, q_{t,N}\}$. To ensure alignment, we select the action with the nearest action-value to R_t as the final action:

$$a_{t,i} = \arg \min_{a_{t,i}} (|q_{t,i} - R_t|). \quad (9)$$

After taking action $a_{t,i}$ and obtaining the reward r_t , we update the desired target return R_{t+1} to $(R_t - r_t)/\gamma$ and repeat the process for the next timestep. This double-check mechanism first ensures that the actions are sampled near the desired target return and then validates them using the action-values to ensure alignment. This mechanism enables the model to interpolate and extrapolate between underrepresented or missing returns in the dataset.

To achieve high returns, we can set an aggressive target return that even exceeds the best possible return. The model will sample actions based on this desired target and validate them with action-values, selecting the action with the highest value. Conversely, to obtain a specific moderate return, we can set that return as the target. The model will then double-check the predicted action, selecting the one with the value closest to the target return. We include the algorithm of *Doctor* in Alg. 1.

4.4. Justification of Double Check Mechanism

To better understand why the proposed double-check mechanism leads to accurate target alignment, we provide a further justification in this section.

Assume our action-value function is optimal, $Q = Q^*$. We select the action a_t that minimizes the absolute difference between the predicted action-value and the desired return according to $a_t = \arg \min_a |Q^*(s_t, a) - R_t|$. We show that this action selection aligns the expected return with R_t , achieving return alignment.

Case 1: $R_t > R$ (desired return exceeds achievable return)

The desired return R_t is greater than the maximum possible return $R = V^*(s_t)$, where:

$$V^*(s_t) = \max_a Q^*(s_t, a) \quad (10)$$

Since $Q^*(s_t, a) \leq V^*(s_t)$ for all actions a , we have:

$$Q^*(s_t, a) - R_t \leq V^*(s_t) - R_t < 0 \quad (11)$$

The absolute difference $|Q^*(s_t, a) - R_t|$ is minimized when $Q^*(s_t, a)$ is maximized. The optimal action a^* is $a^* = \arg \max_a Q^*(s_t, a)$. Selecting $a_t = a^*$

Algorithm 1 Double Checks the Transformer with Target Alignment for Offline RL (*Doctor*)

Input: Sequence buffer \mathcal{D} , Transformer models with weights θ , networks Q with weights ϕ
// Training Phase
for number of training steps $c = 0$ to C **do**
 Sample a batch of length K trajectories $(\dots, R_t, s_t, a_t, r_t)$ from sequence buffer \mathcal{D}
 Update the sum of supervised learning loss and value loss $\mathcal{L}(\theta, \phi)$ via $\mathcal{L}(\theta, \phi) = \mathcal{L}_{\text{recon}}(\theta) + \mathcal{L}_Q(\phi)$.
end for
// Inference Phase
for environment steps $t = 0$ to T **do**
 Initialize the environment $s_0 \leftarrow Env$
 Randomly sample N returns via $\{R_{t,1}, R_{t,2}, \dots, R_{t,N}\} \sim \text{Unif}(\delta(R_t), N)$, and construct N trajectories
 Select the action with the nearest action-value to R_t according to $a_{t,i} = \arg \min_{a_{t,i}} (|q_{t,i} - R_t|)$.
 Execute the action a_t in the environment and observe the reward r_t and next state s_{t+1}
end for

minimizes $|Q^*(s_t, a) - R_t|$. Even when R_t is not attainable, the method selects the action that yields the highest possible return.

Case 2: $R_t < R$ (desired return less than achievable return)

The desired return R_t is less than the maximum possible return $R = V^*(s_t)$. There may exist actions a such that $Q^*(s_t, a) \approx R_t$. By minimizing $|Q^*(s_t, a) - R_t|$, we may select an action a_t where $Q^*(s_t, a_t) \geq R_t$ but potentially less than $V^*(s_t)$. This action aligns the expected return with R_t without necessarily maximizing it and allows for controlled performance.

5. Experiments

In the experiment section, we evaluate *Doctor* across multiple benchmarks to address three questions:

- Can *Doctor* generate actions that achieve closer alignment between actual returns and specified target returns compared to existing baseline methods?
- What is the impact of *Doctor*’s double-check mechanism on target alignment, and how does it translate into improvements in the final performance?
- Can *Doctor* effectively support the policy control requirements in reinforcement learning applications, such as precisely adjusting the skill of the model to flexibly meet the varying treatment objectives in clinical decision-making scenarios?

5.1. Setup

- **Benchmarks.** We use D4RL [15] and EpiCare [5] as our testbeds. D4RL consists of various robotic control environments and datasets. We consider Locomotion-v2 tasks, as well as Maze2D-v1 and Adroit-v1 tasks on the D4RL benchmark. EpiCare is an offline RL benchmark designed for dynamic treatment regimes (DTRs), simulating core challenges in longitudinal clinical settings. It incorporates short treatment horizons, heterogeneous treatment effects, partial observability, and adverse events. The offline dataset used for training is generated through simulated clinical trials, reflecting realistic data collection processes. More environmental details can be found in Appendix C.
- **Baselines.** To address the questions comprehensively, we test our method against representative baselines that are state of the art in each category. We select CQL [23], which adopts pessimistic action estimation. IQN [18], an in-sample multi-step dynamic programming approach. We also include policy regularization-based approaches like TD3+BC [20] as comparison baselines. For RvS-based approaches, we include BC, which maximizes the likelihood of the dataset. DT [12], a transformer-based return conditioned BC, which is shown to be effective on D4RL. And MTM [27] employs a combination of random and autoregressive mask patterns.

5.2. The Superiority of *Doctor* in Return Alignment

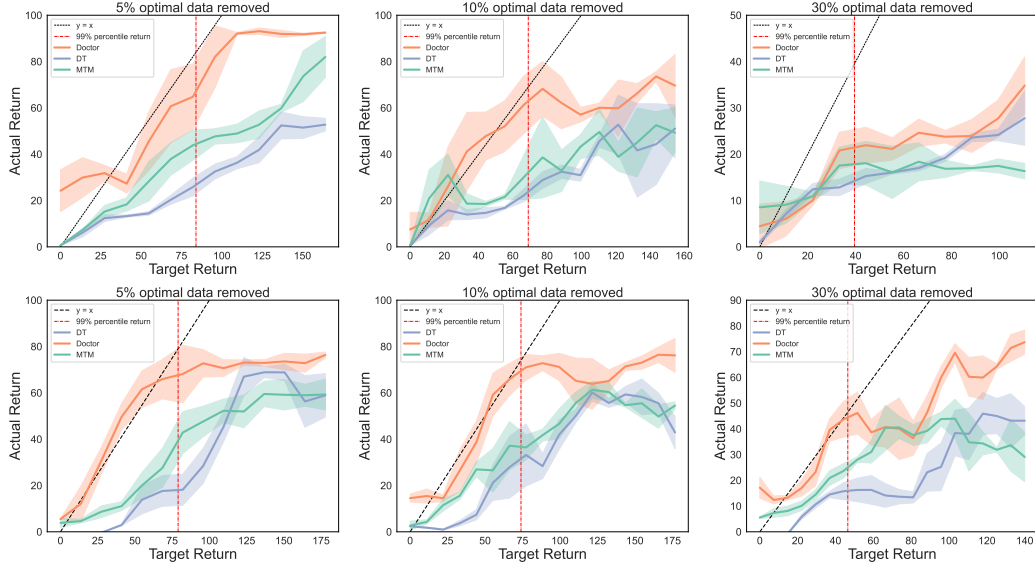


Figure 4: We evaluate the alignment ability of *Doctor* on hopper-medium-replay-v2 (top) and walker2d-medium-replay-v2 (bottom) tasks with the top X% returns of trajectories removed. The dashed red line presents the highest return in the dataset. The dashed black lines denote the ideal alignment. *Doctor* achieves much better alignment across a wide range of target returns compared to DT, MTM.

The key advantage of *Doctor* is its ability to achieve a wide range of desired target returns, an expected capability for return-conditioned models that most existing methods fail to achieve. We first present a visual demonstration to illustrate the efficacy of target alignment achieved by *Doctor*. Specifically, we show the trajectory image recorded on the maze2d-umaze-dense task in Figure 3, providing a more intuitive representation compared to curve-based evaluations.

In this environment, the reward is the exponential negative Euclidean distance between the achieved goal position and the desired goal position:

$$r_t = \exp(-\|g_{\text{achieved},t} - g_{\text{desired}}\|_2), \quad (12)$$

where g_{desired} is the goal position, $g_{\text{achieved},t}$ is the achieved goal position at



Figure 3: Trajectories generated under three different target returns, which are 10, 40 and 80, resulting in actual returns of 37.80, 46.85, and 80.16, respectively, from the left to right. As the target return increases, we observe that the agent is guided closer to the goal.

time step t . The horizon of an episode is 300. We evaluate *Doctor* under three different target returns, specifically 10, 40, and 80, depicted from left to right. The agent is guided to achieve an actual return that aligns with the target return, resulting in actual returns of 37.80, 46.85, and 80.16, respectively. We provide the complete trajectory plots of the agents in Appendix D.

Next, we evaluate the alignment ability of *Doctor* on the hopper-medium-replay-v2 and walker2d-medium-replay-v2 datasets. We vary the level of suboptimality by removing top return trajectories from the dataset and test the model across a wide range of target returns. As suboptimality increases, the maximum returns of the trajectories in the dataset progressively decrease, moving the dataset further away from the optimal.

Figure 4 shows the results. The x-axis represents the target return, the y-axis represents the actual return achieved in the environment. The dashed red line marks the max return in the dataset. The dashed black lines denote the ideal line that perfectly aligns with the target return. *Doctor* achieves significantly better alignment, more closely adhering to the ideal diagonal line, even when the target return exceeds the maximum return in the dataset to some extent. This indicates that *Doctor* can not only interpolate more effectively within the dataset but also facilitates extrapolation, allowing the model to achieve target returns accurately, even beyond those observed in the training data. Notably, bidirectional transformer-based methods like MTM and *Doctor* lie closer to the diagonal than DT, highlighting the architectural advantage in terms of target alignment.

5.3. The Impact of *Doctor*'s Double-Check Mechanism

We further analyze the impact of the sampling size N on the alignment ability of *Doctor* in this section. To investigate this, we conduct an ablation study on hopper-medium-replay-v2 task with 10% of the best data removed, testing N with increasing values in $\{2, 5, 10, 100, 300\}$.

As shown in Figure 5, when $N = 2$, the model utilizes an inference strategy akin to the RvS-based

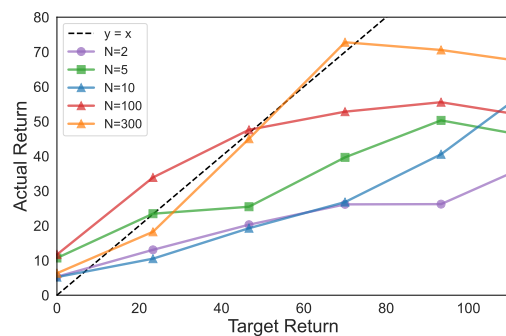


Figure 5: The effect of the sample number N in *Doctor*. As N increases, *Doctor* achieves better alignment with the target return.

method, resulting in inferior alignment. This indicates that the target return alone is not sufficient to ensure alignment. As N increases, the model achieves better alignment, highlighting the importance of multiple samples for target return alignment and the effectiveness of the double-check mechanism. Sampling multiple returns around the target encourages the transformer to propose a rich variety of actions that map the local return, reducing conditioning noise. A subsequent value-function check then filters these candidates, selecting the action whose predicted return most closely matches the target, combining broad exploration with precise validation to achieve substantially tighter alignment.

Time Complexity	DT	MTM	<i>Doctor</i>
Inference (seconds)	0.01	0.012	0.013
Training (seconds)	2.13	1.29	1.35

Table 1: Time Complexity for Algorithms

Approach	halfcheetah-M	hopper-M	walker2d-M
w/o RM	32.3 ± 4.6	14.5 ± 2.4	24.1 ± 6.6
w/o DB	26.2 ± 5.1	12.9 ± 2.7	28.6 ± 7.3
<i>Doctor</i>	16.2 ± 5.8	10.4 ± 3.3	12.0 ± 8.1

Table 2: Absolute error comparison in the ablation study. Results are averaged over three seeds. Lower number is better.

Inducing sampling may introduce extra computational overhead. We evaluate the inference and training time of different algorithms. For training, we use a batch size of 2048 for all four algorithms. We set sizes of hidden units as 256 for all the networks, measuring the time required to train one batch. For inference, we calculate the Frames Per Second (FPS) by running one episode, measuring the total time taken, and then dividing by the episode length. The reported values are the averages of 5 test runs, as shown in Table 1. It can be observed that *Doctor*'s computation overhead does not significantly increase. During inference, *Doctor* processes one batch at a time and leverages a unified architecture to generate both action predictions and value estimates simultaneously, allowing for fully parallel computation. *Doctor* uses a Q function trained with the transformer-based representation, and

Locomotion	BC	CQL	IQL	TD3+BC	DT	MTM	Doctor
halfCheetah-MR	40.2 \pm 1.2	46.1 \pm 0.8	45.4 \pm 1.0	45.6 \pm 0.9	39.1 \pm 1.6	43.0 \pm 1.7	46.6 \pm 0.9
hopper-MR	36.6 \pm 4.6	96.2 \pm 5.2	93.4 \pm 4.9	72.6 \pm 9.4	84.3 \pm 3.5	93.1 \pm 3.4	98.8 \pm 2.1
walker2d-MR	25.3 \pm 8.7	73.5 \pm 1.6	79.5 \pm 2.3	81.8 \pm 1.2	66.0 \pm 3.8	77.3 \pm 2.9	86.2 \pm 2.6
halfCheetah-M	41.8 \pm 1.1	47.0 \pm 0.8	48.1 \pm 0.4	47.2 \pm 0.6	42.0 \pm 1.3	44.1 \pm 0.9	48.4 \pm 0.7
hopper-M	55.7 \pm 5.5	58.5 \pm 4.8	66.2 \pm 3.2	60.3 \pm 6.7	65.2 \pm 3.8	64.9 \pm 3.3	85.6 \pm 7.4
walker2d-M	63.9 \pm 5.9	72.9 \pm 1.5	79.3 \pm 2.4	84.2 \pm 1.6	74.5 \pm 1.3	73.4 \pm 1.7	81.1 \pm 2.7
halfCheetah-ME	55.1 \pm 1.2	91.2 \pm 1.7	89.6 \pm 2.9	92.5 \pm 1.5	86.8 \pm 1.7	94.7 \pm 0.9	95.8 \pm 0.5
hopper-ME	53.2 \pm 4.1	99.5 \pm 10.3	106.7 \pm 6.6	101.2 \pm 8.8	110.6 \pm 1.2	112.4 \pm 0.8	113.5 \pm 0.6
walker2d-ME	100.8 \pm 7.6	109.9 \pm 1.5	109.6 \pm 2.2	111.5 \pm 1.3	108.3 \pm 1.9	111.4 \pm 1.1	113.7 \pm 1.3
Sum	472.6	694.8	717.8	696.9	676.8	714.3	769.7

Table 3: Offline results on the D4RL benchmark. *Doctor* achieves competitive results compared to the baselines, including RvS-based methods and TD learning-based methods. The best baselines are highlighted in bold for final performance.

compared to the computational cost of the transformer itself, the additional cost of Q function computation is relatively low.

Next, we perform an ablation study to quantify the contributions of *Doctor*’s components, random masking and the double-check mechanism on the MuJoCo medium datasets. Table 2 reports the mean absolute error averaged at multiple target returns between the actual return and the target return. When we remove the random-masking pattern (w/o RM), errors rise, indicating that masking is critical to covering a broad return spectrum. Ablating the double-check mechanism (w/o DB) likewise degrades performance, showing its importance for alignment. The full model combining both yields the lowest error across all three tasks.

5.4. The Capability of *Doctor* in Return Maximization

We further assess the return maximization performance of *Doctor* in offline settings, presenting results averaged over five random seeds. As shown in Table 3, *Doctor* outperforms other baselines by a substantial margin and achieves the strongest results in 8 out of 9 tasks on Gym locomotion tasks. *Doctor* integrates supervised learning with TD learning, allowing the model to benefit from the strengths of both paradigms. In datasets with expert-level trajectories such as medium-expert (ME) tasks in the Locomotion environment, *Doctor* performs better than TD learning-based methods like IQL and CQL, demonstrating its ability of sequence modeling. In datasets with medium-level trajectories such as Medium and Medium-Replay, *Doctor*

outperforms RvS-based methods like MTM, and DT, which indicates the stitching capability due to the value functions. This suggests that *Doctor* effectively integrates the advantages of both approaches, achieving superior performance with both low-return and high-return datasets.

Adroit	BC	CQL	IQL	TD3+BC	DT	MTM	Doctor
pen	56.1 ± 13.1	5.4 ± 8.7	83.3 ± 7.3	5.1 ± 4.9	65.2 ± 3.6	80.5 ± 4.2	85.7 ± 8.5
hammer	0.5 ± 0.4	1.9 ± 0.5	3.2 ± 0.6	0.1 ± 0.3	2.0 ± 0.8	5.5 ± 1.1	4.9 ± 3.1
door	0.0 ± 0.0	0.5 ± 0.2	1.8 ± 1.4	0.2 ± 0.2	7.9 ± 2.2	10.5 ± 2.0	9.6 ± 3.2
Sum	56.6	7.8	88.3	5.4	75.1	96.5	100.2

Table 4: Offline results on the Adroit-cloned tasks. *Doctor* achieves competitive or superior results compared to the baselines.

Maze2D	BC	CQL	IQL	TD3+BC	DT	MTM	Doctor
umaze	8.5 ± 7.4	96.0 ± 3.7	44.2 ± 2.9	29.8 ± 11.0	19.0 ± 21.6	26.4 ± 12.1	97.2 ± 9.8
medium	7.1 ± 4.5	80.4 ± 5.6	32.8 ± 3.9	62.1 ± 12.2	28.5 ± 15.7	20.9 ± 7.9	106.2 ± 7.3
large	2.8 ± 0.6	52.1 ± 12.5	63.0 ± 2.9	97.6 ± 13.1	30.4 ± 22.4	41.7 ± 8.0	75.7 ± 6.4
Sum	18.4	228.5	140.0	189.5	77.9	89.0	279.1

Table 5: Offline results on the maze2d tasks. *Doctor* achieves competitive or superior results compared to the baselines.

In addition to evaluation on the locomotion tasks, we further assess *Doctor* in the challenging Adroit tasks, which consist of three dexterous control tasks, each requiring precise interactions and hand-object coordination. As shown in Table 4, *Doctor* outperforms other baselines on the Pen environment, demonstrating *Doctor*'s robustness in these substantially harder high-dimensional dexterous manipulation tasks.

We also evaluate *Doctor* in the Maze2D suite, a classic benchmark for testing an offline agent's ability to stitch together short sub-trajectories into a coherent high-return path. Maze2D comprises three tasks of increasing difficulty (umaze, medium, large). As reported in Table 5, RvS-based approaches (DT, MTM) collapse or do not fully exploit the data. *Doctor* outperforms other baselines including value-based methods that are good at stitching, clearly demonstrating its stitching ability.

These results highlight *Doctor*'s effectiveness in a wide range of tasks.

5.5. The Advantage of Doctor in Clinical Policy Control

In this section, we demonstrate how *Doctor*'s superior alignment can benefit RL applications. To this end, we evaluate *Doctor* using the EpiCare benchmark. EpiCare benchmark provides datasets generated by distinct behavior policies across eight different environments (defined by environment seeds 1–8, each simulating diseases with different characteristics). We use the dataset generated by the Standard of Care (SoC) policy, which simulates clinician behavior by avoiding high-risk treatments based on symptom thresholds. Baseline methods are adapted to discrete control by optimizing logits of one-hot encoded action outputs. We evaluated the models online on 1,000 trajectories, measuring key metrics: clinical returns and adverse events. Clinical returns quantify the overall therapeutic benefit of the treatment policy, while adverse events capture the frequency of unsafe outcomes.

Figure 6 reports clinical return and adverse events per 10k episodes under 0.4 and 0.8 times maximum returns in the datasets. The results demonstrate that (1) DT and MTM exhibit only marginal shifts relative to BC, while *Doctor* shows more significant improvements (improves returns by 22% / 65% and reduces adverse events by 52% / 40% at moderate / aggressive targets compared with BC). (2) DT and MTM have minimal response to target changes. By contrast, *Doctor* can control its policy with treatment aggressiveness, it achieves higher returns at the expense of higher adverse events under aggressive setting, while lower returns but mitigate adverse events under moderate targets.

This result demonstrates that *Doctor* can flexibly control the treatment policy between aggressive and conservative as a single unified model. Such controllability holds promise for clinical practice, allowing physicians to tailor interventions to each patient's unique condition, choosing more aggressive

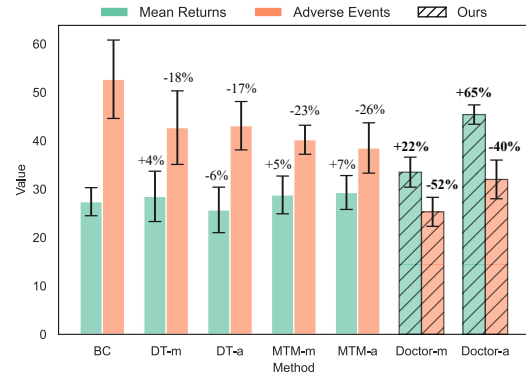


Figure 6: Mean returns and adverse-event rates per 10k episodes under moderate (m, $0.4\times$) and aggressive (a, $0.8\times$) targets. Numbers denote improvement or decrease compared with BC. Results show that (1) DT and MTM exhibit only marginal shifts relative to BC, while *Doctor* demonstrates significant improvements. (2) DT and MTM have minimal responsiveness to target changes. By contrast, *Doctor* can sensitively adjust its policy to meet specified targets.

therapies when potential benefit outweighs risk, or adopting conservative approaches to safeguard vulnerable individuals.

We further report a comparison of *Doctor* against baselines on the EpiCare benchmark in terms of mean returns and adverse event rate on the SoC dataset, as shown in Figure 7. *Doctor* achieves the lowest adverse events and the best clinical returns, outperforming other baselines and demonstrating that *Doctor*’s alignment produces substantially safer and more effective treatment policies on the dynamic treatment regime benchmark.

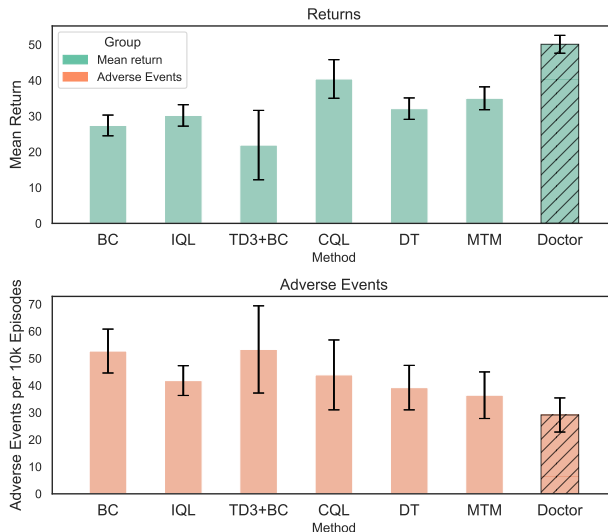


Figure 7: Mean returns and number of adverse events per 10k episodes (lower is better). Results are averaged over eight structurally distinct EpiCare environments (environment seeds 1–8) for each offline learning method on the SoC dataset. Error bars denote standard deviation.

6. Conclusion

This work introduced *Doctor*, a novel offline reinforcement learning approach that integrates a double-check mechanism to enhance target alignment in return-conditioned transformers. By jointly optimizing supervised trajectory reconstruction and temporal-difference value estimation, *Doctor* demonstrates the ability to interpolate across underrepresented return ranges and extrapolate beyond dataset-supported regions. Experimental results on diverse benchmarks, including D4RL and EpiCare, confirm its superiority

over existing methods in both return maximization and controllable policy modulation. These findings highlight the strengths of *Doctor* in balancing therapeutic efficacy with safety in clinical decision-making and in offering fine-grained control in robotics.

At the same time, it is important to recognize the limitations of our study. The evaluation of *Doctor* on medical decision-making tasks remains in a simulated environment, which, although captures many real-world clinical challenges, such as short treatment horizons, heterogeneous treatment effects, partial observability and adverse events, may not fully reflect real-world healthcare data. As a next step, we plan to evaluate our method on real clinical datasets.

Beyond these strengths and weaknesses, our contributions may also benefit current fields. This study focuses on improving the alignment accuracy of RvS methods in offline reinforcement learning. By addressing their current limitations and achieving a closer match between actual and target returns, it advances the field of offline reinforcement learning. The general offline reinforcement learning community may benefit from adopting *Doctor* as a robust baseline. In robotic control, precise alignment between policy outputs and performance targets could enable safer and more reliable manipulation. In healthcare, adaptive treatment planning based on target-aligned policies could support personalized medicine by balancing efficacy and risk. As foundational machine learning research, it poses no negative societal impacts.

Finally, we see promising avenues for future work. A particularly exciting direction is to explore the integration of the double-check mechanism with large foundation models. Recent advances in generative transformers and multimodal learning provide opportunities to incorporate *Doctor*'s target alignment into broader architectures, enabling alignment of outputs with diverse user-defined targets across tasks and modalities. This could, for example, support the development of controllable base models that meet safety, fairness, and performance objectives. Investigating such integration, alongside applying the method to real-world applications, constitutes a vital step for future research.

Appendix A. Outline

In this appendix, we provide the following supporting material in order: Appendix **B** provides further discussion about our architecture design choice; Appendix **C** describes the environment details; Appendix **D** presents extended experimental results such as visualization examples and additional results; and Appendix **E** offers the model and training details.

Appendix B. Additional Discussion for the Design Choice

Transformer Architecture. Early works like DT [12] and TT [13] rely on causal transformers, which predict each subsequent token based on past tokens. Recent studies such as MTM [27] demonstrated that bidirectional transformers trained with a mixture of random and auto-regressive masking achieve good performance. Random masks encourage the model to reconstruct missing tokens by leveraging the context of the unmasked sequence, enhancing the reconstruction and generalization abilities. Our experiments also demonstrate that the bidirectional-based MTM outperforms DT, exhibiting stronger interpolation when handling trajectories associated with underrepresented returns. Our proposed model further enhances these benefits, resulting in improved return alignment.

Q-function Learning. To learn the Q-function, we employ expectile regression [18]. When the expectile parameter $\nu > 0.5$, the resulting loss function assigns lower weight to errors arising from underestimated Q-values. This asymmetric allows us to approximate $Q(s, a) \leftarrow r + \gamma \max_{(s', a') \in \mathcal{D}} Q(s', a')$, achieving reliable in-sample learning. This precision is especially critical for our double-check mechanism, which is dependent on accurate Q-value predictions within data-supported regions, selecting actions closely aligned with the target return.

Appendix C. Environment Details

Appendix C.1. D4RL

Gym Locomotion. The D4RL Gym locomotion benchmark [15] includes environments provided by OpenAI Gym, specifically Walker2d, Hopper, and HalfCheetah. Each task is configured with three levels of dataset difficulty: Medium-Replay, Medium, and Medium-Expert. The Medium dataset corresponds to policies performing at approximately one-third of

expert-level performance, while the Medium-Replay dataset contains the replay buffer from an agent trained to medium-level performance. The Medium-Expert dataset combines trajectories generated by both medium and expert policies. These environments are widely used for evaluating reinforcement learning algorithms. For example, Walker2d environment simulates a robot tasked with walking as fast and as stably as possible. The robot must coordinate its two legs to achieve efficient locomotion without falling over. These environments are designed to test an agent’s ability to learn complex motor skills and optimize control strategies. **Adroit**. Adroit is a suite of dexterous manipulation tasks designed to simulate the control of a five-fingered robotic hand. Our experiments focus on three tasks from this suite: Pen, Door, and Hammer. For example, the Pen task involves rotating a pen to a specific orientation using the robotic hand’s dexterous manipulation skills. The cloned tasks used in our experiment collect a 50-50 split of demonstration data and 2500 trajectories sampled from a behavior cloning policy.

Maze2D. Maze2D is a navigation task in which the agent is required to reach a fixed target position. These tasks are designed to evaluate the ability of offline reinforcement learning algorithms to stitch together different trajectory fragments [15]. We used three environments included in Maze2D, umaze, medium, and large, with complexity and path length to the target increasing sequentially.

Appendix C.2. EpiCare

Environment. EpiCare [5] is a flexible yet clinically motivated benchmark to evaluate offline RL and safety-aware decision making in dynamic treatment regimes. EpiCare frames longitudinal patient care as a finite-horizon POMDP. The hidden state space $S = \{s_r, s_a, s_1, \dots, s_{n_s}\}$ contains n_s disease states plus terminal remission (s_r) and adverse event (s_a) states, the discrete action set $A = \{a_1, \dots, a_{n_a}\}$ represents treatments, and the observation space $O = [0, 1]^{d_o}$ records d_o separate symptoms that the clinician sees. Disease progression obeys a transition function T that is multiplicatively modulated by each treatment’s vector m_a , together with treatment-specific remission probabilities $T(s_r | s_i, a)$ and an observation-triggered adverse-event rule, this yields the transition function:

$$T(s_j | s_i, a) = (1 - T(s_r | s_i, a) - T(s_a | s_i, a)) \frac{(m_a)_j T_{i,j}}{\sum_k (m_a)_k T_{i,k}}. \quad (C.1)$$

Observations are generated by adding a treatment-specific symptom shift δ_a to a state-dependent Gaussian draw \tilde{o} , then applying: $o = [\text{expit}(\tilde{o} + \delta_a)]_1$, capturing measurement noise and treatment side effects. The reward function is

$$R(s, a, o) = \begin{cases} r_r, & s = s_r \\ r_a, & s = s_a \\ -c_a - c_o \sum_i o_i, & \text{otherwise} \end{cases} \quad (\text{C.2})$$

where $r_r > 0$ rewards remission, $r_a = -r_r$ penalizes adverse events, c_a encodes treatment cost and c_o prices symptom cost. An episode starts from an initial distribution derived from the stationary mix of the Markov graph and ends in remission, an adverse event, or after a maximum of treatment steps. Each random environment seed automatically instantiates new state graphs, symptom distributions, and treatment parameters.

Behavior Policy. The Standard-of-Care (SoC) policy seeks immediate benefit while avoiding harm, which is used to collect data on the EpiCare benchmark in our experiment. The SoC policy emulates a risk-averse clinician who ignores the hidden disease state and instead tracks the instantaneous value of each treatment as a multi-armed bandit. It resets the estimate to the expected reward $Q_0(a) = \mathbb{E}[R | a]$, then updates it after each dose with an exponentially recency-weighted rule

$$Q_{t+1}(a) = \begin{cases} Q_t(a) + \alpha (R_t - Q_t(a)), & a = a_t \\ Q_t(a), & a \neq a_t \end{cases}, \quad (\text{C.3})$$

To protect the patient, SoC greedily selects the reward-maximising action within the safe set $A_{\text{safe}}(o) = \{a \in A : (\delta_a)_i \leq 0 \text{ for all } i \text{ with } o_i \geq 1 - \frac{\kappa}{2}\}$, thereby refusing any drug that would further elevate a symptom already above the danger threshold κ .

Appendix D. Additional Experimental Results

Appendix D.1. Visualization Example for Return Alignment

In this section, we provide an intuitive toy demonstration to illustrate the efficacy of return alignment achieved by *Doctor*. We record the gif on the maze2d-umaze-dense task. The Maze2D dataset contains suboptimal trajectories and is specifically designed to evaluate the stitching ability. Supervised learning-based methods, such as DT, struggle when faced with suboptimal

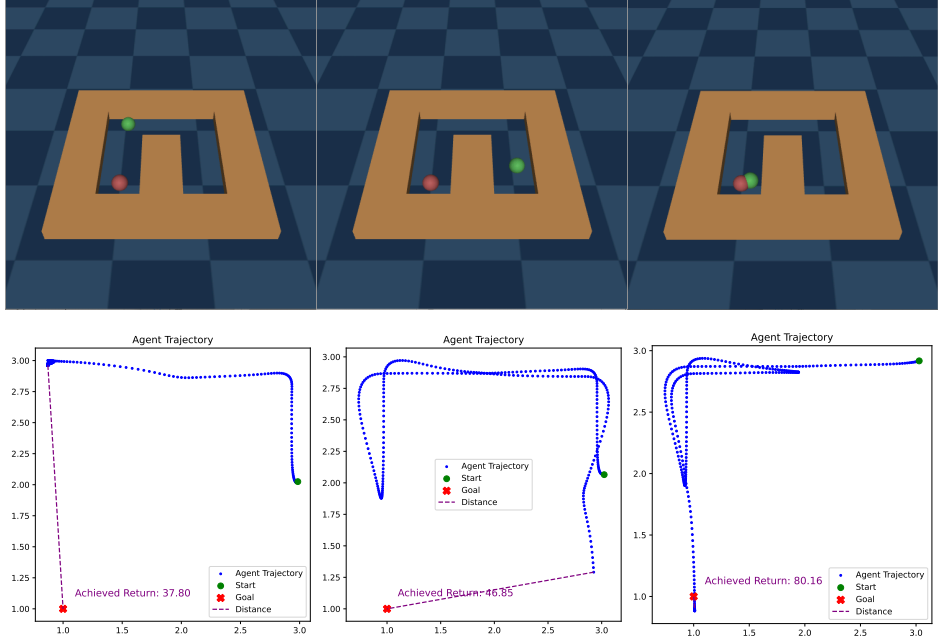


Figure C.8: Trajectories generated under three different target returns, which are 10, 40 and 80, respectively, from the left to right. The first row shows the frames near the end of the trajectories, while the second row displays the corresponding trajectories produced by the inference model. As the target return increases, we observe that the agent is guided closer to the goal

trajectories. As a reference, the normalized return of *DT* in this environment is -6.8, indicating a complete collapse in performance [28].

We save the model parameter of *Doctor* trained offline and evaluate in this environment, where each rollout is limited to 300 steps. We present trajectories generated under three different target returns. The first row of Figure C.8 shows the frames near the end of the trajectories, while the second row displays the corresponding trajectories produced by the inference model. As the target return increases, we observe that the agent is guided closer to the goal. For example, when the target return is 80, the agent is closer to the goal than when the target return is 40. In this environment, since the reward is the exponential negative Euclidean distance between the achieved goal position and the desired goal, even if the agent remains stationary, it will still receive a positive return. Interestingly, when the target return is 40, the ball exhibits higher acceleration compared with the target return of 10, traveling further, while the actual return is controlled to achieve the target

return precisely. When the target return is 80, the ball ultimately chooses to achieve a higher return and reaches the place near the goal.

Appendix D.2. Additional Results for Online Finetuning

Locomotion Tasks	IQL	MTM-O	ODT	<i>Doctor</i>
HalfCheetah-MR	44.2 → 44.5	43.0 → 43.4	40.0 → 41.2	46.6 → 42.4 \pm 0.9
Hopper-MR	94.7 → 97.5	92.9 → 94.6	86.6 → 91.3	98.8 → 98.6\pm2.0
Walker2d-MR	73.9 → 79.2	77.3 → 82.1	68.9 → 78.4	86.2 → 88.5\pm5.4
HalfCheetah-M	47.4 → 47.1	43.6 → 45.2	42.7 → 43.6	48.4 → 44.3 \pm 1.8
Hopper-M	66.3 → 80.1	64.1 → 70.2	66.9 → 98.1	85.6 → 93.5 \pm 5.1
Walker2d-M	78.3 → 81.9	70.4 → 71.0	72.2 → 77.0	81.1 → 84.7\pm3.7
Sum	404.8 → 430.3	391.3 → 406.5	377.3 → 429.6	446.7 → 452.0

Table D.6: Online fine-tuning results. We report the average returns after 1 million online interactions. *Doctor* observes clear improvements on Hopper-M.

In this section, we further investigate whether the double-check mechanism can help the base transformer model to explore novel states in the environment for fine-tuning, thereby boosting performance. During online exploration, actions are sampled based on a desired target return, indicating the area we wish to explore. The Q function then evaluate these actions, providing prior knowledge about potential actions. For example, we can select actions from the Boltzmann distribution based on the Q function,

$$\pi(a_t | s_t) = \frac{\exp(\beta q_{t,i})}{\sum_i \exp(\beta q_{t,i})}, \quad (\text{D.1})$$

where β is a temperature parameter that controls the sharpness of the distribution.

This results in an effective exploration strategy that integrates prior knowledge from the value functions and the desired target returns.

We evaluate this in an online setting, aimed to test whether the model can further improve by interacting with the environment. We maintain the top 5% of the trajectories in the dataset and further interact with the environment for 1 million steps, which corresponds to approximately 1500 episodes. We sample actions based on Eq. D.1 and set target returns dynamically as the maximum return R_{\max} in the dataset and $\delta = 2R_{\max}$, $\beta = 100$. Each time after rolling out for one episode, we perform 200 gradient updates based on the collected data.

As shown in Table D.6, *Doctor* achieves a performance improvement on some tasks when incorporating additional online interaction data. ODT [39] is a DT-based variant trained with sequence-level entropy regularization for offline-to-online fine-tuning. MTM-O is an online variant of MTM we implement for test its ability of fintuning. *Doctor* outperforms ODT and IQL in several tasks, with clear improvements in performance on Hopper-M. This demonstrates the effectiveness of the double-check mechanism for online fine-tuning, allowing the model to explore effectively. The availability of online data can further improve the performance of transformer models.

Appendix E. Model and Training Details

We build our policy and Q value heads as a transformer-based model. The detailed model hyperparameters are in Table D.7. For baselines, we train the model using the setting inherited from CORL [40].

We provide implementation details of *Doctor*. The supervised learning model include a bidirectional transformer encoder and a bidirectional transformer decoder. Before inputting the sequence data into the model, each input modality is projected into the embedding space through independent embed-encodings. The output of the decoder is connected to a 2-layer MLP with layer normalization, which is used to reconstruct the trajectory sequence. The Transformer is trained with a randomly sampled series of mask ratios similar to [27]: $\text{mask_ratios} = [0.6, 0.7, 0.8, 0.85, 0.9, 0.95, 1.0]$. For data sampling, we adopt a two-step sampling method similar to that used in DT [12], where we first sample a single trajectory and then uniformly sample sub-trajectories of a certain sequence length.

For offline training, we perform 140,000 gradient updates during training, and evaluate the model by rolling out 10 episodes. we set $N = 300$ and δ is small value fluctuating based on the maximum return in the dataset. Specifically, we choose $\delta = 5\% \times R_{\max}$.

We initialize the AdamW optimizer for the Transformer model and the Adam optimizer for the Q-value head, employing both warmup and decay schedules. The Q-value head consists of two 256-dimensional MLP layers, which connect to the output of the transformer decoder. All hyperparameters are summarized in Table D.7. We report the final results over five random seeds.

During the fine-tuning stage, we initialize the replay buffer with the top 5% highest-return trajectories from the offline dataset. Each time we interact

Transformer Policy	Value
Encoder layers	2
Decoder layers	1
Activation function	GeLu
Number of attention heads	4
Embedding dimension	512
layers of decoding head	2
Dropout	0.10
Positional encoding	Yes
Dropout	0.1
Learning rate	0.0001
Weight decay	0.005
Betas	[0.9,0.999]
Learning rate warmup steps	20000
<i>Q</i> Value Heads	Value
Number of layers	2
Activation function	ReLU
Embedding dimension	256
Tau	0.7 (Locomotion), 0.9 (Maze2d), 0.8 (Adroit and EpiCare)
Learning rate	0.0001
Weight decay	5e-4
General	Value
Eval episodes	10
Input trajectory length	4
Trainning steps	140000
Batch size	512
Discount factor	0.99

Table D.7: Hyperparameters of *Doctor* in experiments

with the environment, we fully roll out one episode using the current policy and add it to the replay buffer. We then update the policy and roll out again, following a process similar to [39].

References

- [1] S. Levine, A. Kumar, G. Tucker, J. Fu, Offline reinforcement learning: Tutorial, review, and perspectives on open problems, arXiv preprint arXiv:2005.01643 (2020).
- [2] Z. Liu, Y. Zhuang, P. Wu, Y. Liu, Iris: An information path planning method based on reinforcement learning and information-directed sampling, Pattern Recognition 172 (2026) 112400. doi:<https://doi.org/10.1016/j.patcog.2025.112400>.
- [3] H. Chen, R. Yang, J. Zhang, X. Wen, Y. Chen, D. Yu, C. Bai, Z. Wang, Temporal consistent multi-view perception for robust embodied manipulation, Pattern Recognition 171 (2026) 112177. doi:<https://doi.org/10.1016/j.patcog.2025.112177>.
- [4] B. Jiang, S. Chen, Q. Zhang, W. Liu, X. Wang, Alphadrive: Unleashing the power of vlms in autonomous driving via reinforcement learning and reasoning, arXiv preprint arXiv:2503.07608 (2025).
- [5] M. Hargrave, A. Spaeth, L. Grosenick, Epicare: A reinforcement learning benchmark for dynamic treatment regimes, Advances in Neural Information Processing Systems 37 (2024) 130536–130568.
- [6] S. Choi, S. Jang, S. Jung, H. J. Cho, B. Jeon, Deep reinforcement learning for efficient registration between intraoral-scan meshes and ct images, Pattern Recognition 164 (2025) 111502. doi:<https://doi.org/10.1016/j.patcog.2025.111502>.
- [7] T. Pang, G. Wu, Y. Zhang, B. Wang, Y. Yin, Qfae: Q-function guided action exploration for offline deep reinforcement learning, Pattern Recognition 158 (2025) 111032. doi:<https://doi.org/10.1016/j.patcog.2024.111032>.
- [8] L. H. Goetz, N. J. Schork, Personalized medicine: motivation, challenges, and progress, Fertility and sterility 109 (6) (2018) 952–963.
- [9] A. Singla, A. N. Rafferty, G. Radanovic, N. T. Heffernan, Reinforcement learning for education: Opportunities and challenges, arXiv preprint arXiv:2107.08828 (2021).

- [10] H. A. Alawwad, A. Alhothali, U. Naseem, A. Alkhathlan, A. Jamal, Enhancing textual textbook question answering with large language models and retrieval augmented generation, *Pattern Recognition* 162 (2025) 111332. doi:<https://doi.org/10.1016/j.patcog.2024.111332>.
- [11] H.-C. Jeon, I.-C. Baek, C.-m. Bae, T. Park, W. You, T. Ha, H. Jung, J. Noh, S. Oh, K.-J. Kim, Raidenv: Exploring new challenges in automated content balancing for boss raid games, *IEEE Transactions on Games* (2023).
- [12] L. Chen, K. Lu, A. Rajeswaran, K. Lee, A. Grover, M. Laskin, P. Abbeel, A. Srinivas, I. Mordatch, Decision transformer: Reinforcement learning via sequence modeling, *Advances in neural information processing systems* 34 (2021) 15084–15097.
- [13] M. Janner, Q. Li, S. Levine, Offline reinforcement learning as one big sequence modeling problem, *Advances in neural information processing systems* 34 (2021) 1273–1286.
- [14] S. Emmons, B. Eysenbach, I. Kostrikov, S. Levine, Rvs: What is essential for offline rl via supervised learning?, *arXiv preprint arXiv:2112.10751* (2021).
- [15] J. Fu, A. Kumar, O. Nachum, G. Tucker, S. Levine, D4rl: Datasets for deep data-driven reinforcement learning, *arXiv preprint arXiv:2004.07219* (2020).
- [16] A. Kumar, J. Fu, M. Soh, G. Tucker, S. Levine, Stabilizing off-policy q-learning via bootstrapping error reduction, *Advances in Neural Information Processing Systems* 32 (2019).
- [17] R. S. Sutton, A. G. Barto, *Reinforcement learning: An introduction*, MIT press, 2018.
- [18] I. Kostrikov, A. Nair, S. Levine, Offline reinforcement learning with implicit q-learning, in: *International Conference on Learning Representations*, 2022.
URL <https://openreview.net/forum?id=68n2s9ZJWF8>

- [19] H. Zhang, C. Xiao, C. Gao, H. Wang, M. Müller, et al., Exploiting the replay memory before exploring the environment: enhancing reinforcement learning through empirical mdp iteration, *Advances in Neural Information Processing Systems* 37 (2024) 85658–85692.
- [20] S. Fujimoto, S. S. Gu, A minimalist approach to offline reinforcement learning, *Advances in neural information processing systems* 34 (2021) 20132–20145.
- [21] J. Wu, H. Wu, Z. Qiu, J. Wang, M. Long, Supported policy optimization for offline reinforcement learning, *Advances in Neural Information Processing Systems* 35 (2022) 31278–31291.
- [22] H. Zhang, C. Xiao, H. Wang, J. Jin, bo xu, M. Müller, Replay memory as an empirical MDP: Combining conservative estimation with experience replay, in: *The Eleventh International Conference on Learning Representations*, 2023.
URL <https://openreview.net/forum?id=SjzFVSJUt8S>
- [23] A. Kumar, A. Zhou, G. Tucker, S. Levine, Conservative Q-learning for offline reinforcement learning, *Advances in Neural Information Processing Systems* 33 (2020) 1179–1191.
- [24] H. Liu, P. Abbeel, Emergent agentic transformer from chain of hindsight experience, in: *International Conference on Machine Learning*, PMLR, 2023, pp. 21362–21374.
- [25] Y.-H. Wu, X. Wang, M. Hamaya, Elastic decision transformer, in: *Proceedings of the 37th International Conference on Neural Information Processing Systems*, 2023, pp. 18532–18550.
- [26] Y. Chebotar, Q. Vuong, K. Hausman, F. Xia, Y. Lu, A. Irpan, A. Kumar, T. Yu, A. Herzog, K. Pertsch, et al., Q-transformer: Scalable offline reinforcement learning via autoregressive q-functions, in: *Conference on Robot Learning*, PMLR, 2023, pp. 3909–3928.
- [27] P. Wu, A. Majumdar, K. Stone, Y. Lin, I. Mordatch, P. Abbeel, A. Rajeswaran, Masked trajectory models for prediction, representation, and control, in: *International Conference on Machine Learning*, PMLR, 2023, pp. 37607–37623.

- [28] T. Yamagata, A. Khalil, R. Santos-Rodriguez, Q-learning decision transformer: Leveraging dynamic programming for conditional sequence modelling in offline rl, in: International Conference on Machine Learning, PMLR, 2023, pp. 38989–39007.
- [29] C.-X. Gao, C. Wu, M. Cao, R. Kong, Z. Zhang, Y. Yu, Act: empowering decision transformer with dynamic programming via advantage conditioning, in: Proceedings of the AAAI Conference on Artificial Intelligence, Vol. 38, 2024, pp. 12127–12135.
- [30] Y. Wang, C. Yang, Y. Wen, Y. Liu, Y. Qiao, Critic-guided decision transformer for offline reinforcement learning, in: Proceedings of the AAAI Conference on Artificial Intelligence, Vol. 38, 2024, pp. 15706–15714.
- [31] J. Kim, S. Lee, W. Kim, Y. Sung, Adaptive q -aid for conditional supervised learning in offline reinforcement learning, Advances in Neural Information Processing Systems 37 (2024) 87104–87135.
- [32] T. Tanaka, K. Abe, K. Ariu, T. Morimura, E. Simo-Serra, Return-aligned decision transformer, arXiv preprint arXiv:2402.03923 (2024).
- [33] K. He, X. Chen, S. Xie, Y. Li, P. Dollár, R. Girshick, Masked autoencoders are scalable vision learners, in: Proceedings of the IEEE/CVF conference on computer vision and pattern recognition, 2022, pp. 16000–16009.
- [34] X. Li, Y. Zheng, H. Chen, X. Chen, Y. Liang, C. Lai, B. Li, X. Xue, Instruction-guided fusion of multi-layer visual features in large vision-language models, Pattern Recognition 170 (2026) 111932. doi:<https://doi.org/10.1016/j.patcog.2025.111932>.
- [35] J. Xia, X. Zhu, B. Jiang, S. Kan, Reasoning elicitation and multi-granularity contrastive learning for text-rich image understanding in large vision-language models, Pattern Recognition 171 (2026) 112278. doi:<https://doi.org/10.1016/j.patcog.2025.112278>.
- [36] A. Vaswani, Attention is all you need, Advances in Neural Information Processing Systems (2017).

- [37] W. K. Newey, J. L. Powell, Asymmetric least squares estimation and testing, *Econometrica: Journal of the Econometric Society* (1987) 819–847.
- [38] A. Huang, Y. Wang, R. Liu, H. Zou, X. Zhou, Qvf: Incorporating quantile value function factorization into cooperative multi-agent reinforcement learning, *Pattern Recognition* 161 (2025) 111323. doi:<https://doi.org/10.1016/j.patcog.2024.111323>.
- [39] Q. Zheng, A. Zhang, A. Grover, Online decision transformer, in: international conference on machine learning, PMLR, 2022, pp. 27042–27059.
- [40] D. Tarasov, A. Nikulin, D. Akimov, V. Kurenkov, S. Kolesnikov, Corl: Research-oriented deep offline reinforcement learning library, *Advances in Neural Information Processing Systems* 36 (2024).